Mutual Impedance Computation of a Waveguide Slot-Fed Arbitrary Patch Using Combined Conventional Moment Method and Equivalent Electric and Magnetic Dipole Method

Mehri Hoseini[1], Keyvan Forooraghi[1, *], and Ali Abdolali[2]

Abstract—This paper proposes computing the mutual impedance of a multi-layer patch fed by a slotted waveguide using the combined equivalent electric and magnetic dipole-moment method and conventional moment method (EDM-MOM) as an efficient technique. The slot, PEC, and dielectric regions are substituted with equivalent currents. The unknown currents are expanded using the Rao-Wilton-Glisson and Schaubert-Wilton-Glisson basis functions. The matrix equations are then extracted from the boundary conditions. Using the EDM, each RWG or SWG of the PEC and dielectric is equivalent to an infinitesimal electric dipole, and that of the slot is equivalent to a magnetic dipole. The element matrix related to the waveguide excitation is calculated using the conventional moment method due to simple integration and accuracy. Further, the superposition of the mutual coupling between each equivalent electric or magnetic dipole in the first element and each dipole in the second element is used to obtain the mutual impedance of the two elements of the waveguide slot-fed patch array. The proposed method shows good agreement with CST software simulation results.

1. INTRODUCTION

Patch arrays are attractive structures because of their compact size and low cost and have found applications in radar and satellite communication systems and phased array antenna. However, they show low gains at high frequencies. Combining patch arrays with a slotted waveguide can resolve the issue [1–4]. An accurate array design requires considering the mutual coupling between array components. In designing waveguide slot arrays via the Elliot method, analytical expressions are used to calculate the coupling impedance [5].

The method of moments is a common analysis method for the arbitrary shape patch antenna [6]. In the case of patch arrays, integral equations are obtained for unknown surface currents by applying boundary conditions [7, 8]. The equations are solved using the method of moments in the frequency domain, and the mutual impedance is determined accordingly. The volume integral equation (VIE) analyzes dielectric structures with inhomogeneous materials [9–12]. Due to the heavy computations required to solve VIEs, surface integral equations are also proposed for these structures [13–15]. In previous research [16], a comparison was performed between the results obtained by surface and volume integral equations in analyzing dielectric resonators. Combined surface-volume integral equations are employed to take advantage of inhomogeneous dielectrics analysis via volume integrals and reduce the computations of surface integrals [17–20]. In this paper, we have also formulated the combined surface-volume integral equations.

Method of moments with Schaubert-Wilton-Glisson (RWG) and Schaubert-Wilton-Glisson (SWG) basis functions has been studied in structures such as slots, patch antennas, and substrate-integrated

* Corresponding author: Keyvan Forooraghi (keyvan_f@modares.ac.ir).
[1] Department of Electrical and Computer Engineering, Tarbiat Modares University, Tehran, Iran. [2] Department of Electrical Engineering, Iran University of Science and Technology, Tehran, Iran.

waveguides (SIWs) in [21–23]. These basis functions efficiently analyze patch antennas with arbitrary configurations such as conformal patch antennas [24]. Probe feed is often proposed in such structures, and the equivalent source is electrical. The integral equations in analyzing the structures with magnetic sources are demonstrated in [25]. A rectangular patch coupled with the slotted waveguide was analyzed using the method of moments with sine basis functions in [26]. For the first time, the analysis of an arbitrary patch fed by a slotted waveguide based on RWG and SWG basis functions is investigated in this paper. In the current paper, we have combined field integral equations (CFIEs) because, at the slot position, the magnetic field integral equation (MFIE) is applied due to the magnetic boundary condition. Moreover, electric field integral equations (EFIEs) are applied in the remaining part of the PEC and dielectrics.

Modeling the antenna with equivalent dipoles is a straightforward technique for reducing the computations in analyzing the antenna [27–30]. In this paper, we have used the equivalent dipole method to simplify the calculation of the moment matrix elements. Also, the matrix terms of the equivalent dipole method are obtained for a waveguide slot-fed patch antenna. As the second innovation, the analysis based on the combined method of moments with RWG and SWG basis functions and the equivalent dipole method is employed. Therefore, unlike the previous methods, the matrix elements are computed based on a combination method of the equivalent dipole method and a conventional moment method. In the proposed method, to calculate the matrix element related to excitation, the moment method is used to reduce the error. Meanwhile, the equivalent dipole method is used to calculate other matrix elements because of its simplicity and speed. Accordingly, less memory and simpler calculations are required than in the moment method alone, and higher accuracy is obtained than in the equivalent dipole method alone. The superposition of the fields in the dipoles of the first element and all dipoles in the second element is employed to calculate the mutual coupling.

The first objective of this paper is to analyze the coupling of the arbitrary patch coupled with a slotted waveguide. The reason for following this aim is the importance of calculating coupling in the design of arrays. Therefore, in this paper, the boundary condition equations of the arbitrary patch coupled with the slot are obtained, and the matrix of the moment method is formed using the expansion of currents with the RWG and SWG basis functions. Regarding the antenna's relatively large size, the matrix element relationships for the equivalent dipole method are obtained to reduce the computational memory. The second purpose of this paper is to minimize the error due to the approximation of waveguide excitation with equivalent dipoles. For this purpose, matrix elements related to waveguide excitation are calculated without approximation with equivalent dipoles. This term is computed by using the conventional moment method, which has less error than the equivalent dipole method. Since the equivalent dipole method is an approximation of the moment method, the error of the combined moment method-equivalent dipole is expected to be lowered than the equivalent dipole method alone. The results of this paper have confirmed the prediction.

The paper's organization is as follows. In Section 2, we provide the formulation for the moment method. In addition, electric and magnetic currents are expanded via RWG and SWG basis functions, and the derived boundary condition equations are arranged into a matrix form. Section 3 focuses on applying the equivalent dipole method. The mutual impedance calculation between the two elements of an array of the waveguide slot-fed is described in Section 4. Section 5 discusses the results and compares them with CST software simulation results. Finally, Section 6 summarizes the main findings of the paper.

2. FORMULATION

This section uses the moment method to analyze the waveguide slot-fed arbitrary patch antenna. For this purpose, the boundary condition equations are written in slots, dielectrics, and patches based on the moment method. Therefore, the equivalent surface electric currents in the patches, the equivalent volumetric electric currents in the dielectrics, and the equivalent magnetic current of the slots are expanded with the RWG and SWG basis functions. The expanded currents are substituted in the boundary condition equations. Then, the equations are written in matrix form by dot product to the corresponding test functions, which are the RWG and SWG basis functions. The equivalent dipole method can reduce the complexity of the matrix calculations. This method calculates the moment of

equivalent dipoles of RWG and SWG elements. In expressions related to matrix elements, instead of using the free space Green function (according to the conventional moment method), matrix elements are calculated using infinitesimal dipole field equations. The equivalent dipole method formulation for a patch coupled with a slotted waveguide is one of the novelties of this paper. In addition, a combination of the moment method and the equivalent dipole method is proposed to reduce the error compared to the equivalent dipole method. In other words, the matrix element related to excitation is obtained without equivalent dipole approximation and by integrating the relationships of waveguide excitation fields. The difference between the proposed method and the equivalent dipole method is that the latter employs a field of an infinitesimal equivalent dipole as an approximation instead of using the Green function inside the waveguide. In this work, the matrix elements related to the Green function inside the waveguide are calculated using the usual moment method. The other elements of the matrix, which are calculated from the free space Green function in the conventional moment method, are approximated by infinitesimal dipole fields. The arbitrary waveguide-fed patch is shown in Fig. 1. There is a longitudinal slot. Further, a multilayer patch antenna exists on top of the slot. The shape of the patch antenna, the number of dielectric layers, and their characteristic parameters are arbitrary.
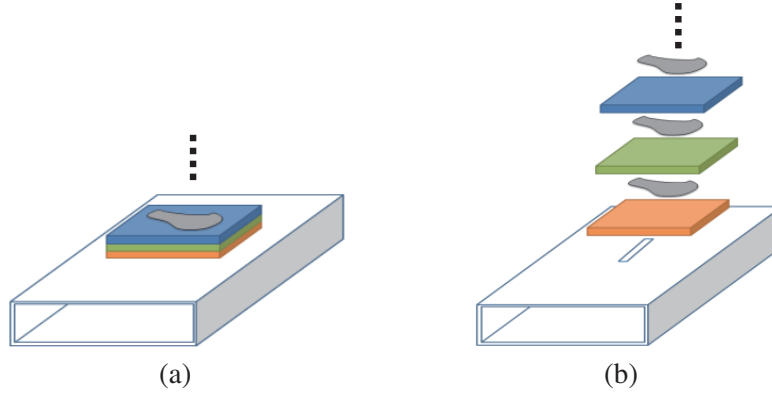
Figure 1. Geometry of the arbitrary waveguide-fed patch. (a) Waveguide slot-fed patch antenna. (b) Constituent layers.

2.1. Boundary Conditions

It is unnecessary to write the boundary equations separately in each dielectric [31]. Thus Eq. (1) is written for all dielectric regions (ε_d is variable). Moreover, Eq. (2) is correct for the PEC surface everywhere in the antenna. Regarding the notations of currents, $\vec{J}_p$ is used for the surface equivalent current densities in the perfect electric conductor (PEC) (patches and waveguide walls). In addition, $\vec{J}_d$ denotes the volume equivalent current densities in the first and second dielectric mediums, and M_s is the equivalent magnetic current in the slot. Additionally, $\vec{D}$ indicates the electric flux density in dielectric mediums and is an unknown parameter. $\vec{E}_p^s(\vec{U})$ and $\vec{E}_d^s(\vec{U})$ refer to the induced electric field on PEC and dielectric due to the source $\vec{U}$, respectively, where $\vec{U} \in \{\vec{J}_p, \vec{J}_d, M_s\}$. Concerning the magnetic fields inside the slot, $H_{M_s}^s(\vec{U})$ denotes the induced magnetic field due to source current $\vec{U}$, and H^{inc} represents the incident magnetic field. ε_d is the dielectric permittivity.

- Over the dielectric mediums

$$\frac{\vec{D}}{\varepsilon_d} - \vec{E}_d^s\left(\vec{J}_p\right) - \vec{E}_d^s\left(\vec{J}_d\right) - \vec{E}_d^s\left(\vec{M}_s\right) = 0 \tag{1}$$

- Over the PEC surfaces

$$\vec{E}_p^s\left(\vec{J}_p\right) + \vec{E}_p^s\left(\vec{J}_d\right) + \vec{E}_p^s\left(\vec{M}_s\right) = 0 \tag{2}$$

- Over the slot surface

$$\vec{H}_{M_s}^s\left(\vec{J}_p\right) + \vec{H}_{M_s}^s\left(\vec{J}_d\right) + \vec{H}_{M_s}^s\left(\vec{M}_s\right) = \vec{H}^{inc} \tag{3}$$

2.2. Expansion of Electric and Magnetic Currents

The dielectric medium and PEC are discretized into tetrahedral volume and triangle surface elements, respectively. Next, the volume/surface equivalent current densities are expanded over the PEC, dielectric, and slot. Eq. (4) demonstrates the relation between $\vec{D}$ and $\vec{J}_d$. The RWG basis function is suitable for the surface current. Moreover, in the case of volume equivalent currents, the SWG basis function is used as follows [32]:

$$\vec{D}(\vec{r}) = \sum_{n=1}^{N_D} D_n^D \vec{f}_n^v(\vec{r}), \quad \vec{J}_d(\vec{r}) = j\omega K(\vec{r}) \vec{D}(\vec{r}), \quad K(\vec{r}) = \frac{\hat{\varepsilon}(\vec{r}) - \varepsilon_o}{\hat{\varepsilon}(\vec{r})} \tag{4}$$

$$\vec{J}_p(\vec{r}) = \sum_{n=1}^{N_v} I_n^p \vec{f}_n^p(\vec{r}) \tag{5}$$

$$\vec{M}_s = \sum_{n=1}^{N_v} V_m^{Ms} \vec{f}_m^{Ms}(\vec{r}) \tag{6}$$

where $\vec{f}_n^p$ and $\vec{f}_m^{Ms}$ are the RWG basis functions for the equivalent surface electric and magnetic currents in the PEC and slot, respectively, and $\vec{f}_n^v$ denotes the SWG basis function for the equivalent volume electric currents in dielectric mediums. The details of these basis functions can be found in previous studies [31, 33]. In addition, $\hat{\varepsilon}(\vec{r})$ is the relative dielectric permittivity in two dielectrics, and ε_0 represents the electric permittivity in the free space.

2.3. Matrix Equations

Using the dot products of the expanded currents in Eqs. (1) to (3) to their corresponding basis functions, these equations are rewritten in a matrix form, and the relation is expressed for each matrix element. Concerning Eqs. (1) to (3) and the detailed derivation of the matrix elements in [32], we have:

$$\begin{bmatrix} Z^{DD} & Z^{PD} & C^{M_sD} \\ Z^{DP} & Z^{PP} & C^{M_sP} \\ T^{DM_s} & T^{PM_s} & Y^{M_sM_s} \end{bmatrix} \begin{bmatrix} D^D \\ I^P \\ V^{Ms} \end{bmatrix} = \begin{bmatrix} 0 \\ 0 \\ I^i \end{bmatrix} \tag{7}$$

$$Z_{mn}^{DD} = \left\langle \vec{f}_m^v, \vec{f}_n^v/(j\omega\varepsilon) \right\rangle - \left[\left\langle \vec{f}_m^v, E\left(\vec{f}_n^v\right) \right\rangle \right] \tag{8}$$

$$Z_{mn}^{PD} = \left[\left\langle \vec{f}_m^v, E\left(\vec{f}_n^p\right) \right\rangle \right] \tag{9}$$

$$Z_{mn}^{DP} = \left[\left\langle \vec{f}_m^p, E\left(\vec{f}_n^v\right) \right\rangle \right] \tag{10}$$

$$Z_{mn}^{PP} = \left[\left\langle \vec{f}_m^p, E\left(\vec{f}_n^p\right) \right\rangle \right] \tag{11}$$

$$C_{mn}^{MsD} = \left[\left\langle \vec{f}_m^v, E\left(\vec{f}_n^{Ms}\right) \right\rangle \right] \tag{12}$$

$$C_{mn}^{MsP} = \left[\left\langle \vec{f}_m^p, E\left(\vec{f}_n^{Ms}\right) \right\rangle \right] \tag{13}$$

$$Y_{mn}^{M_sM_s} = \left[\left\langle \vec{f}_m^{Ms}, H\left(\vec{f}_n^{Ms}\right) \right\rangle \right] \tag{14}$$

$$T_{mn}^{DM_s} = \left[\left\langle \vec{f}_m^{Ms}, H\left(\vec{f}_n^v\right) \right\rangle \right] \tag{15}$$

$$T_{mn}^{PM_s} = \left[\left\langle \vec{f}_m^{Ms}, H\left(\vec{f}_n^p\right) \right\rangle \right] \tag{16}$$

2.4. Integral Computations inside the Waveguide

In matrix Eq. (7), $I^i = \langle \vec{f}_m^{Ms}, H^{inc} \rangle$, and H^{inc} is obtained from the Green's function of the fields inside a slotted waveguide. In a waveguide with the dominant mode TE10, the field equations are as in [34].

According to RWG basis function definition ($\vec{f}_m^{Ms}$) [33], we can write

$$
I_i = \int\limits_{T_n^+ + T_n^-} \vec{f}_m^{Ms} \{\hat{n} \times H_i(r)\} \, dS
$$

$$
= \phi \int\limits_{T_n}^{+} \frac{L_n}{2A_n^+} (\vec{r} - \vec{r}_n^+) \left[\frac{\pi}{a} \left(\frac{e^{\frac{j\pi x}{a}} + e^{-\frac{j\pi x}{a}}}{2} \right) \hat{a}_z + j\beta_g \left(\frac{e^{\frac{j\pi x}{a}} - e^{-\frac{j\pi x}{a}}}{2j} \right) \hat{a}_x \right] e^{-j\beta_g z} dx dz
$$

$$
+ \phi \int\limits_{T_n}^{-} \frac{L_n}{2A_n^-} (\vec{r} - \vec{r}_n^-) \left[\frac{\pi}{a} \left(\frac{e^{\frac{j\pi x}{a}} + e^{-\frac{j\pi x}{a}}}{2} \right) \hat{a}_z + j\beta_g \left(\frac{e^{\frac{j\pi x}{a}} - e^{-\frac{j\pi x}{a}}}{2j} \right) \hat{a}_x \right] e^{-j\beta_g z} dx dz \tag{17}
$$

$$
I_i = \frac{\beta_g \phi}{2} \frac{L_n}{2A_n^+} \left[\int\limits_{T_n}^{+} x e^{\frac{j\pi x}{a}} dx - \int\limits_{T_n}^{+} x e^{\frac{-j\pi x}{a}} dx - \int\limits_{T_n}^{+} x_n e^{\frac{j\pi x}{a}} dx + \int\limits_{T_n}^{+} x_n e^{\frac{-j\pi x}{a}} dx \right] \int\limits_{T_n}^{+} e^{-j\beta_g z} dz
$$

$$
+ \frac{\pi\phi}{2a} \frac{L_n}{2A_n^+} \left[\int\limits_{T_n}^{+} z e^{-j\beta_g z} dz \cdot \int\limits_{T_n}^{+} e^{\frac{j\pi x}{a}} dx + \int\limits_{T_n}^{+} z e^{-j\beta_g z} dz \cdot \int\limits_{T_n}^{+} e^{\frac{-j\pi x}{a}} dx - \int\limits_{T_n}^{+} z_n e^{-j\beta_g z} dz \cdot \int\limits_{T_n}^{+} e^{\frac{j\pi x}{a}} dx \right.
$$

$$
\left. - \int\limits_{T_n}^{+} z_n e^{-j\beta_g z} dz \cdot \int\limits_{T_n}^{+} e^{\frac{-j\pi x}{a}} dx \right] + \frac{\beta_g \phi}{2} \frac{L_n}{2A_n^-} \left[\int\limits_{T_n}^{-} x e^{\frac{j\pi x}{a}} dx - \int\limits_{T_n}^{-} x e^{\frac{-j\pi x}{a}} dx - \int\limits_{T_n}^{-} x_n e^{\frac{j\pi x}{a}} dx \right.
$$

$$
\left. + \int\limits_{T_n}^{-} x_n e^{\frac{-j\pi x}{a}} dx \right] \int\limits_{T_n}^{-} e^{-j\beta_g z} dz + \frac{\pi\phi}{2a} \frac{L_n}{2A_n^-} \left[\int\limits_{T_n}^{-} z e^{-j\beta_g z} dz \cdot \int\limits_{T_n}^{-} e^{\frac{j\pi x}{a}} dx + \int\limits_{T_n}^{-} z e^{-j\beta_g z} dz \cdot \int\limits_{T_n}^{-} e^{\frac{-j\pi x}{a}} dx \right.
$$

$$
\left. - \int\limits_{T_n}^{-} z_n e^{-j\beta_g z} dz \cdot \int\limits_{T_n}^{-} e^{\frac{j\pi x}{a}} dx - \int\limits_{T_n}^{-} z_n e^{-j\beta_g z} dz \cdot \int\limits_{T_n}^{-} e^{\frac{-j\pi x}{a}} dx \right] \tag{18}
$$

Given that $\int x e^{\frac{j\pi x}{a}} dx = (\frac{a}{j\pi})^2 [\frac{j\pi}{a} x e^{\frac{j\pi x}{a}} - e^{\frac{j\pi x}{a}}]$, these integrals can be computed using the numerical Gaussian quadrature integration for triangles [35].

3. METHOD OF EQUIVALENT DIPOLES

The element matrix I^i in Eq. (7) is related to the waveguide excitation calculated in Section 2.4 due to simple integration and accuracy without needing the equivalent dipole method. This section applies the equivalent dipole method for the other elements to reduce the problem complexity and computation time due to double integration.

3.1. Deriving of Equivalent Dipole-Moments

On a PEC surface, the equivalent electric dipole moment corresponding to the nth element of RWG (denoted by m_{es} in this paper) can be obtained by integrating its surface current over the surface of that element according to [32]. The nth dipole-moment of SWG (denoted by m_{ev}) is also obtained by integrating the volume current over the volume of that element [32, 36]. The equivalent magnetic dipole moment is obtained as follows:

$$
m_{hs} = \int\limits_{T_n^+ + T_n^-} M_{sn}(r') \, ds' = I_{sn} m_{hsn} \tag{19}
$$

$$
m_{hsn} \approx l_{hn} \left(r_n^{c-} - r_n^{c+} \right) \tag{20}
$$

3.2. The Electric and Magnetic Fields of Equivalent Dipoles

The electric and magnetic fields of the mth infinitesimal electric dipole are expressed in [37]. According to the duality theorem [38], the fields of the equivalent infinitesimal magnetic dipoles within the slot are obtained by:

$$E_{hn}(r) = -\frac{jk}{4\pi}(m_{hn} \times r) Ce^{-jkr}, \quad C = \frac{1}{r^3}\left[1 + \frac{1}{jkr}\right] \tag{21}$$

$$H_{hn}(r) = \frac{1}{4\pi\eta}\left((M_{hn} - m_{hn})\left[C + \frac{jk}{r}\right] + 2M_{hn}C\right)e^{-jkr}, \quad M_{hn} = \frac{(r \cdot m_{hn})r}{r^2} \tag{22}$$

where m_{hn} denotes the magnetic dipole moment. These equations are accurate; they are valid for near and far-field estimations.

3.3. Calculation of Matrix Elements Using Equivalent Dipole Fields

To reduce the complexity in Eqs. (8) to (16) and according to equations in [32], the scattered field of the nth element of RWG and SWG is substituted with the field of the equivalent dipole in the following equations, where indices "en" and "hn" are for electric dipole and magnetic dipole fields, respectively. Additionally, the "h" index (l_{hm}) differentiates the common edge length of magnetic currents.

$$Z_{mn} = \begin{cases} -l_m[e^{-jkR}E_{en}(R)|_{R=|r'_m-r'_n|} \cdot \left(r_m^{C-} - r_m^{C+}\right) & T_m^{\pm} \in S \\ -a_m[e^{-jkR}E_{en}(R)|_{R=|r'_m-r'_n|} \cdot \left(r_m^{C-} - r_m^{C+}\right) & T_m^{\pm} \in V \\ -a_m[e^{-jkR}E_{en}(R)|_{R=|r'_m-r'_n|} \cdot \left(r_{ms}^{C} - r_m^{C+}\right) & T_m^{+} \in V, \ T_m^{-} \notin V \end{cases} \tag{23}$$

$$C_{mn} = \begin{cases} -l_m[e^{-jkR}E_{hn}(R)|_{R=|r'_m-r'_n|} \cdot \left(r_m^{C-} - r_m^{C+}\right) & T_m^{\pm} \in S \\ -a_m[e^{-jkR}E_{hn}(R)|_{R=|r'_m-r'_n|} \cdot \left(r_m^{C-} - r_m^{C+}\right) & T_m^{\pm} \in V \\ -a_m[e^{-jkR}E_{hn}(R)|_{R=|r'_m-r'_n|} \cdot \left(r_{ms}^{C} - r_m^{C+}\right) & T_m^{+} \in V, \ T_m^{-} \notin V \end{cases} \tag{24}$$

$$Y_{mn} = -l_{hm}[e^{-jkR}H_{hn}(R)|_{R=|r'_m-r'_n|} \cdot \left(r_m^{C-} - r_m^{C+}\right) \quad T_m^{\pm} \in S \tag{25}$$

$$T_{mn} = -l_{hm}[e^{-jkR}H_{en}(R)|_{R=|r'_m-r'_n|} \cdot \left(r_m^{C-} - r_m^{C+}\right) \quad T_m^{\pm} \in S \tag{26}$$

4. COMPUTATION OF THE MUTUAL IMPEDANCE

It is assumed that the electric and magnetic currents, (J_1, K_1) and (J_2, K_2), produce electromagnetic fields (E_1, H_1) and (E_2, H_2) in patches 1 and 2, respectively. According to the reaction theorem in [39], the mutual impedance due to the currents of antenna 1 in antenna 2 is obtained via

$$Z_{21} = -\frac{1}{I_{11}I'_{22}}\int_{V_2} (J_2 \cdot E_1 - K_2 \cdot H_1)dv \tag{27}$$

As noted in [40], we can obtain the electric and magnetic currents in a dipole array via

$$J_2(r, r') = \sum_{n=1}^{N_d} J^n\delta(r - r'_n), \quad K_2(r, r') = \sum_{n=1}^{N_h} M^n\delta(r - r'_n) \tag{28}$$

where J^n is the nth electric dipole, and M^n denotes the nth magnetic dipole. N_d is the total number of equivalent electric dipoles, and N_h is the total number of equivalent magnetic dipoles. According to these equations, the following expressions can be written for an array of magnetic and electric dipoles [41]:

$$Z_{ij} = \frac{1}{I_iI_j}\sum_{n=1}^{N_{dj}} E_i^d(r'_n) \cdot J_j^n - \frac{1}{I_iI_j}\sum_{n=1}^{N_{hj}} H_i^d(r'_n) \cdot M_j^n \tag{29}$$

where $E_i^d(r'_n)$ and $H_i^d(r'_n)$ are electric and magnetic fields due to all the electric dipoles of the ith cell of the array at position r'_n, respectively. Moreover, J_j^n and M_j^n represent the dipole-moment of the

nth array element of the jth cell array. Based on the superposition theorem, the mutual impedance between the two cells i and j equals the sum of the mutual impedance due to each dipole in cells i and j. Substituting the total field of all dipoles in Eq. (29), we have:

$$Z_{ij} = \frac{1}{I_i I_j} \sum_{n=1}^{N_{dj}} \sum_{m=1}^{N_i} E_i^{dm}(r'_n) \cdot J_j^n - \frac{1}{I_i I_j} \sum_{n=1}^{N_{hj}} \sum_{m=1}^{N_i} H_i^{dm}(r'_n) \cdot M_j^n \tag{30}$$

where N_i is the total number of dipoles in element i of the array, $r'_n = \frac{r_n^{c+} + r_n^{c-}}{2}(r_n^{c+}$, and r_n^{c-} is the distance between the centroid of the triangles constituting the nth edge element and the origin).

5. RESULTS

As mentioned earlier, the patch shape and dielectric layers could be arbitrary. The waveguide slot-fed patch is demonstrated in Fig. 2. The waveguide dimensions are 22.86 mm and 10.16 mm (WR90 type). There is a longitudinal slot with a width of 1.58 mm. On top of the slot, there is a dielectric medium with a relative permittivity $\varepsilon r = 2.64$, which is commercially available in substrate Rogers RO4725JXR. The cross-sectional dimensions are 11 mm $\times$ 33 mm, and the height of $h1$ is 2.62 mm. On this layer, the first patch composed of the same square pixel patches with the size of 1.1 mm is illustrated in Fig. 2(a). A dielectric medium (FR4) with the size of 11 mm $\times$ 33 mm and a height of 1.36 mm is laid above the
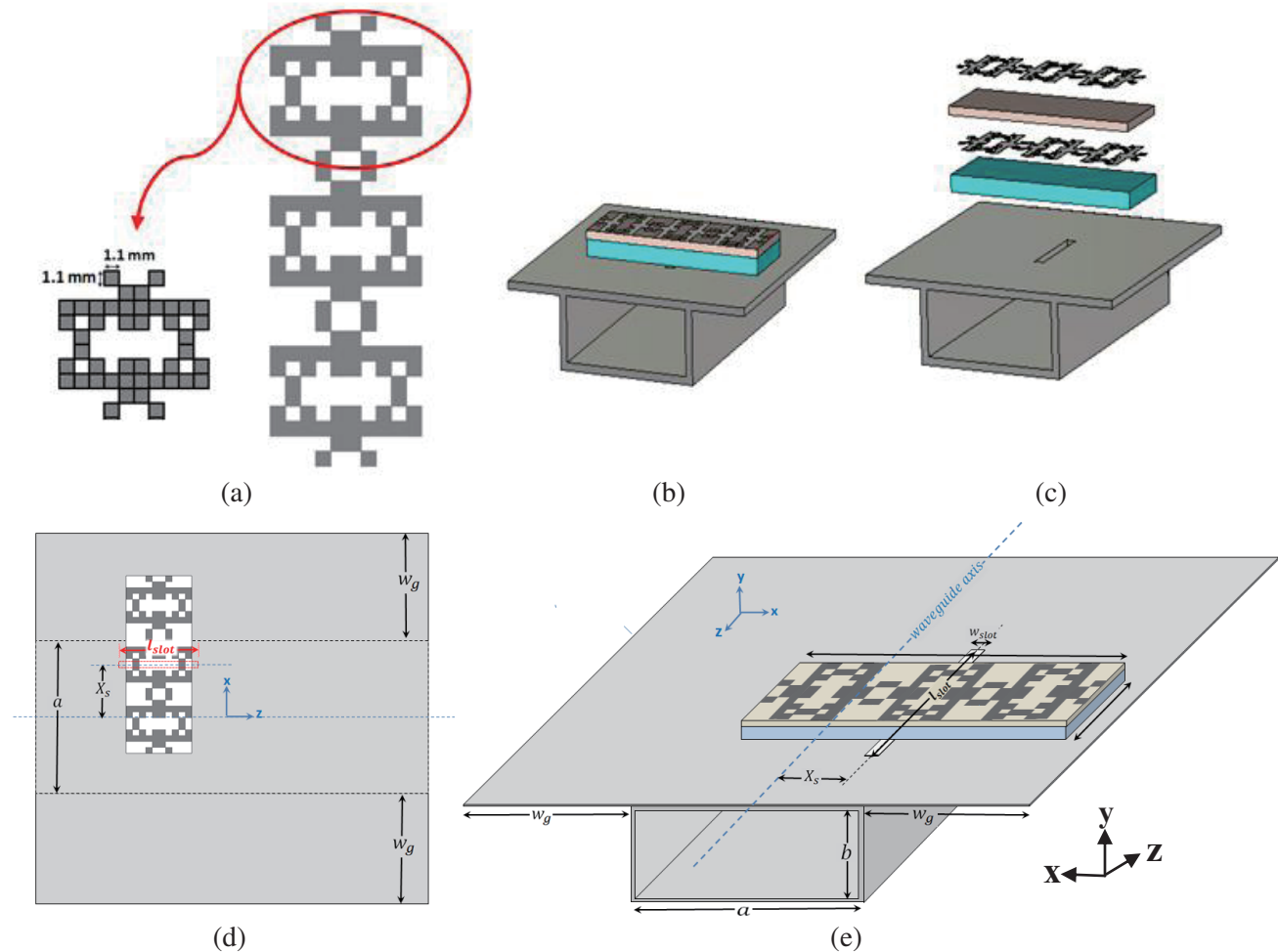
Figure 2. Geometry of the waveguide-fed patch. (a) Patch antenna. (b) Waveguide slot-fed patch antenna. (c) Constituent layers. (d) Top view. (e) 3D view.

patch. Finally, another identical patch is placed on the dielectric medium (FR4). X_s is the offset of the slot center from the waveguide axis, and the patch offset with respect to the slot is zero in this paper. $a + 2w_g$ is the dimension of the square ground of the patch on top of the waveguide. l_{sot} (slot length) is equal to 16.96 mm for resonance in the frequency of 9.5 GHz, and w_{slot} (slot width) equals 1.58 mm in all cases. The position of the patch relative to the slot is constant in all cases. The patch and slot centers are in the same place. In other words, no matter how much the slot offset changes, the patch is moved by the same amount. Fig. 2(a) is obtained by connecting components consisting of square pixels with dimensions of 1.1 mm × 1.1 mm at the resonant frequency of 9.5 GHz using genetic algorithm optimization. In this procedure, the algorithm examines the different states of the presence or absence of pixels. The optimization variables are the number of pixels and each pixel's presence or absence (0 and 1). Also, the objective function is the resonance at the desired frequency.

In the present paper, the structure of Fig. 3 is suggested for calculating the mutual impedance of the two elements by using CST software (time domain solver) to validate the results. As shown, there is a PEC box between the two waveguides. The distance between each slot and the feed point is $\lambda_g/2$. Additionally, the distance between each slot and the short circuit is $\lambda_g/4$. The PEC box in the middle is used to adjust the distance between the two slots and compute the coupling variations due to slot dislocations.
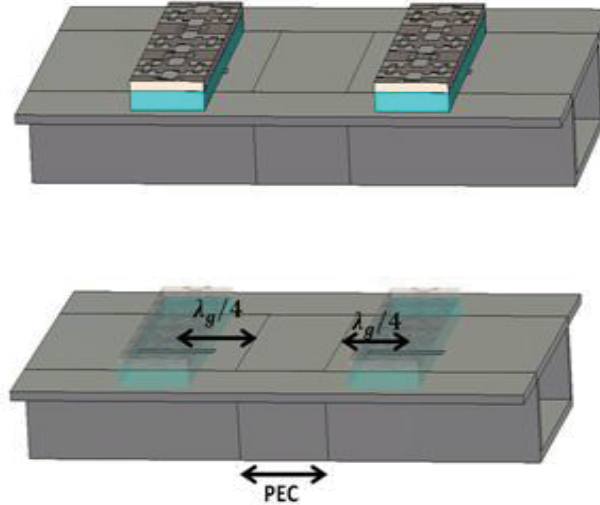
Figure 3. The model used to obtain mutual impedance of proposed elements.

Figures 4, 5, and 6 show the mutual impedance when the two slots have the same length for offsets 1–4 mm and collinear, parallel, and parallel displaced situations for the two elements (the left side of the figures). For each offset, the results are obtained for the associated resonant length of that slot. According to the data, increasing the offset leads to coupling enhancements.

The distance between one peak and the next peak in real and imaginary diagrams of the mutual impedance is about λ. As expected, at intervals where the maximum or minimum of the real part occurs, the imaginary part curve becomes 0. Regarding offsets smaller than 1 mm, the coupling is small. Thus, we can ignore coupling in the design of arrays with a small offset. However, the amount of coupling cannot be ignored in large offsets. In the linear case, the slots form an H-plane array; the coupling rapidly decreases by increasing the distance. Each λ increase in distance in a linear slot causes the real and imaginary parts of the coupling impedance to be almost halved. Therefore, in the design of large arrays, the coupling of elements far from each other can be ignored. In contrast, for the parallel case, we have an E-plane array; thus, decreasing coupling due to increasing the distance happens at a slower rate. In parallel slots, by increasing the distance as much as λ, the real and imaginary parts of the coupling impedance decreases less than that in the linear case. This result indicates that in the linear case, the coupling depends more on the distance of the slots. For instance, let us consider a linear array with 20 elements with equal distances of 0.5λ and assume the same offset of 2 mm for all elements.
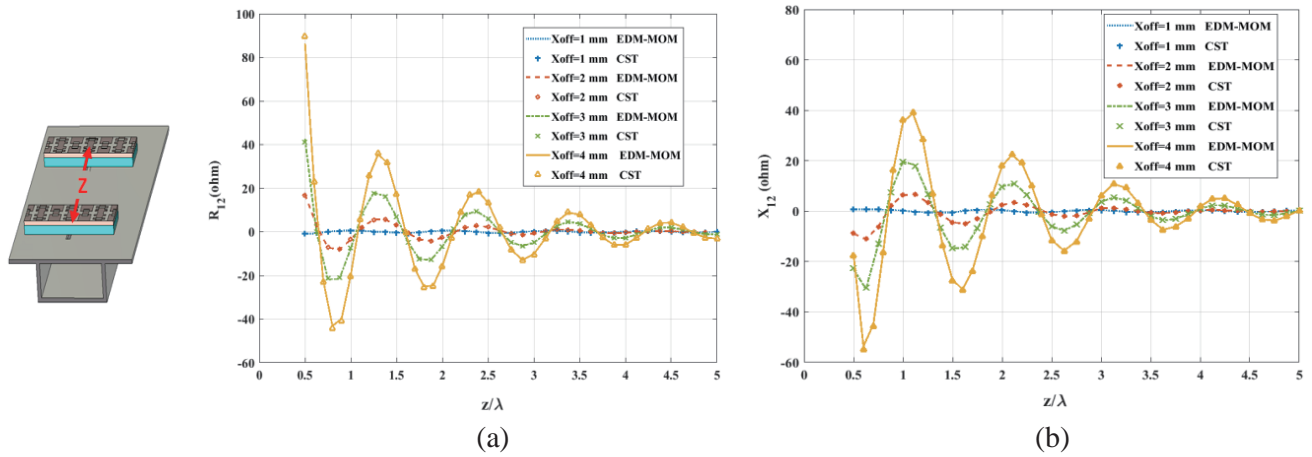
Figure 4. (a) Real and (b) Imaginary part of coupling impedance for two collinear slots.
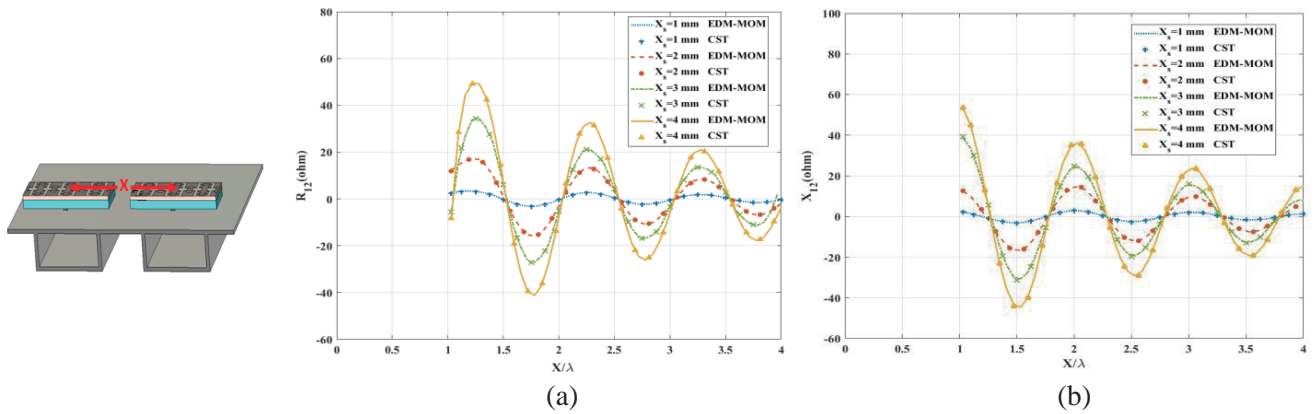
Figure 5. (a) Real and (b) Imaginary part of coupling impedance for two Parallel slots.
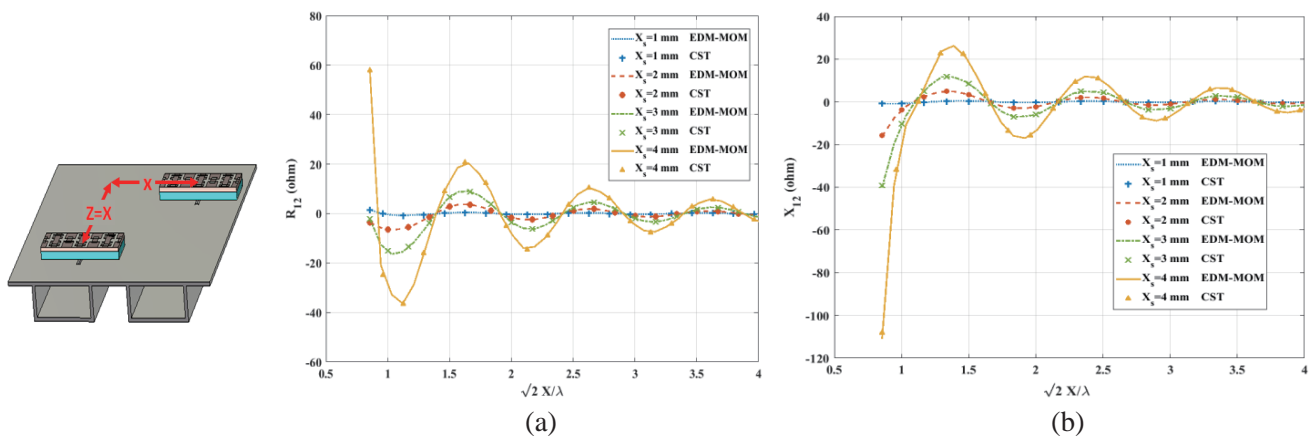
Figure 6. (a) Real and (b) Imaginary part of coupling impedance for two parallel displaced slots.

According to the red diagram of Figure 4(a), the coupling of the first element with other elements can be calculated by ignoring the coupling of the first element with the eighth element onwards (elements 8 to 20) (that are spaced more than 4λ).

Table 1. Comparison of this work to conventional methods.

	CST	MOM	EDM	This work (EDM-MOM)
Time (s)	2902	1146	478	633
CPU (Mb)	744	1647	364	423
Accuracy (%)	3.08		3.36	1.87

Table 1 compares the proposed combined conventional moment method and EDM (EDM-MOM) and the previous methods. We have investigated 50 random samples of the variables of element spacing, how the two elements are juxtaposed (i.e., linear, parallel, and parallel displaced), and their offsets. The error is defined as follows:

$$Error = \left(\frac{1}{N} \sum_{n=1}^{N} \left| \left(\frac{Z_{\text{EDM-MOM}} - Z_{\text{MOM}}}{Z_{\text{MOM}}} \right) \right| \right) \times 100\% \tag{31}$$

In this equation, N is the number of samples of the moment method compared with the proposed EDM-MOM method, $Z_{\text{EDM-MOM}}$ the mutual impedance calculated from the proposed method, and Z_{MOM} the mutual impedance calculated from the MOM method. The average error of these 50 random samples is considered in the error calculation. The total number of elements in CST is 167,832 (two collinear slots, $Z = 0.5\lambda$). In the moment method, the number of triangles is 1658, and the number of tetrahedrons is 5916. The element matrix details for the conventional moment method are derived according to equations in [25]. The integrals are calculated according to Gaussian quadrature formulas in [42] and in singular cases, based on the method in [43]. The accuracy is calculated assuming MOM data as the reference. The recommendation for validation is to make a simulation using a method from a different family. The conventional moment method, the equivalent dipole, and the proposed combined methods are all based on the equivalent currents. Therefore, the CST software results (time-domain solver) are used for validation. But simulation with CST is time-consuming, especially in large arrays. So it is not recommended in the design process of the arrays, and we have used it here only to validate the proposed method. We aim to obtain a method based on the moment method, which gives values closer to the moment method than the equivalent dipole method. Therefore, the reference is classical MoM. A processor with a 2.50 GHz CPU speed is used in all cases. Based on the results, the proposed method's computation time and required memory are much better than the conventional moment method and CST software results, and better accuracy with little extra time and memory is obtained than EDM.

A comparison of the proposed method with similar previous works is presented in Table 2. According to Table 2, this method's most important advantage is improving the maximum computational error while maintaining simplicity and relatively short time of computations.

Table 2. Comparison of this work to references.

System	RAM	Computation time (s)	Number of Elements	Maximum Error	Method
No Information	low	261	3163	5%	EDM [44]
Intel-Core i7-CPU at 3.40 GHz with 32 GB of RAM	High (20 GHz)	1680	No Information	No Information	MOM [23]
Intel-Core i7-CPU at 2.5 GHz with 8 GB RAM	Low (423 Mb)	633	7574	1.9%	This work (EDM-MOM)

6. CONCLUSION

In this paper, combined conventional moment method and equivalent dipole-moment method were applied to compute the mutual impedance of the two elements of the waveguide slot-fed arbitrary patch antenna arrays. According to the surface and volume equivalence theorem, dielectrics and patches were substituted with the corresponding volume and surface equivalent currents. In addition, a magnetic current modeled the slot. The boundary conditions for PEC, dielectrics, and slots were obtained, and then unknown currents were expanded via RWG and SWG basis functions using the moment method. Next, equivalent electric and magnetic dipole moments for the triangles and tetrahedrons were calculated to reduce the computing time and complexity. After computing the matrix elements using the fields of equivalent dipoles and solving the equations, the mutual coupling versus the distance between the two elements was evaluated for different positions and offsets of the two slots. Comparing the results obtained by the proposed approach with the simulation results of CST showed that the proposed method led to less complexity in analysis and computed mutual impedances with sufficient accuracy.

REFERENCES

1. Ho, M. H., K. A. Michalski, and K. Chang, "Waveguide excited microstrip patch antenna-theory and experiment," *IEEE Transactions on Antennas and Propagation*, Vol. 42, No. 8, 1114–1125, 1994.

2. Ho, M.-H. and C.-I. G. Hsu, "Circular-waveguide-fed microstrip patch antennas," *Electron. Lett.*, Vol. 41, 1202, 2005.

3. Wu, W., J. Yin, and N. Yuan, "Design of an efficient X-band waveguide-fed microstrip patch array," *IEEE Transactions on Antennas and Propagation*, Vol. 55, No. 7, 1933–1939, 2007.

4. Hwang, J. and Y. Oh, "Millimeter-wave waveguide slot-array antenna covered by a dielectric slab and arrayed patches," *IEEE Antennas and Wireless Propagation Letters*, Vol. 8, 1050–1053, 2009.

5. Elliott, R. S., *Antenna Theory and Design*, Prentice-Hall, Englewood Cliffs, NJ, 1981.

6. Harrington, R. F., *Field Computation by Moment Methods*, Macmillan, New York, 1968.

7. Pan, S. G. and I. Wolff, "Computation of mutual coupling between slot-coupled microstrip patches in a finite array," *IEEE Transactions on Antennas and Propagation*, Vol. 40, No. 90, 1047–1053, 1992.

8. Fang, D. G., C. Z. Luan, and Y. P. Xi, "Mutual coupling in microstrip antenna array: Evaluation, reduction, correction or compensation," *IEEE International Workshop on Antenna Technology: Small Antennas and Novel Metamaterials*, 37–40, 2005.

9. Ozdemir, N. A. and J. F. Lee, "IE-FFT algorithm for a non conformal volume integral equation for electromagnetic scattering from dielectric objects," *IEEE Transactions on Magnetics*, Vol. 44, 1398–1401, 2008.

10. Guo, J. L., J. Y. Li, and Q. Z. Liu, "Analysis of arbitrarily shaped dielectric radomes using adaptive integral method based on volume integral equation," *IEEE Transactions on Antennas and Propagation*, Vol. 54, 1910–1916, 2006.

11. Nie, X. C., L. W. Li, N. Yuan, T. S. Yeo, and Y. B. Gan, "A fast volume-surface integral equation solver for scattering from composite conducting-dielectric objects," *IEEE Transactions on Antennas and Propagation*, Vol. 53, 818–824, 2005.

12. Nie, X. C., L. W. Li, N. Yuan, T. S. Yeo, and Y. B. Gan, "Precorrected-FFT solution of the volume integral equation for 3-D inhomogeneous dielectric objects," *IEEE Transactions on Antennas and Propagation*, Vol. 53, 313–320, 2005.

13. Liu, Y., S. Safavi-Naeini, S. K. Chaudhuri, and R. Sabry, "On the determination of resonant modes of dielectric objects using surface integral equations," *IEEE Transactions on Antennas and Propagation*, Vol. 52, No. 4, 1062–1069, 2004.

14. Glisson, A. W., D. Kajefez, and J. James, "Evaluation of modes in dielectric resonators using a surface integral equation formulation," *IEEE Trans. Microwave Theory Tech.*, Vol. 31, No. 12, 1023–1029, 1983.

15. Rao, S. M., T. K. Sarkar, P. Midya, and A. R. Djordevic, "Electromagnetic radiation and scattering from finite conducting and dielectric structures: Surface/surface formulation," *IEEE Transactions on Antennas and Propagation*, Vol. 39, 1034–1037, 1991.

16. Liu, Y., S. Safavi-Naeini, and S. K. Chaudhuri, "Comparison of SIE-MoM and VIE-MoM for determination of complex resonant frequency of dielectric resonators," *IEEE Antennas Propag. Int. Symp.*, 641–644, Columbus, Ohio, June 2003.

17. Lu, C. C. and W. C. Chew, "A coupled surface-volume integral equation approach for the calculation of electromagnetic scattering from composite metallic and material targets," *IEEE Transactions on Antennas and Propagation*, Vol. 48, No. 12, 1866–1868, 2000.

18. Yucel, A. C., L. J. Gomez, and E. Michielssen, "Internally combined volume-surface integral equation for EM analysis of inhomogeneous negative permittivity plasma scatterers," *IEEE Transactions on Antennas and Propagation*, Vol. 66, No. 4, 1903–1913, 2018.

19. Gomez, L. J., A. C. Yücel, and E. Michielssen, "Internally combined volume-surface integral equation for a 3-D electromagnetic scattering analysis of high-contrast media," *IEEE Antennas and Wireless Propagation Letters*, Vol. 16, 1691–1694, 2017.

20. Gomez, L. J., A. C. Yücel, and E. Michielssen, "Low-frequency stable internally combined volume-surface integral equation for high-contrast scatterers," *IEEE Antennas and Wireless Propagation Letters*, Vol. 14, 1423–1426, 2015.

21. Makarov, S., "MoM antenna simulation, with Matlab: RWG basis function," *IEEE Antennas and Propagation Magazin*, Vol. 43, No. 5, 100–107, October 2001.

22. Makarov, S. N., S. D. Kulkarni, A. G. Marut, and L. C. Kempel, "Method of moments solution for a printed patch/slot antenna on a thin finite dielectric substrate using the volume Integral equation," *IEEE Transactions on Antennas and Propagation*, Vol. 54, No. 4, 1174–1184, 2006.

23. Bertrand, M., G. Valerio, M. Ettorre, and M. Casaletti, "RWG basis functions for accurate modeling of substrate integrated waveguide slot-based antennas," *IEEE Transactions on Magnetics*, Vol. 56, No. 1, 1–4, Art. No. 6700204, January 2020.

24. Yuan, N., T. S. Yeo, X.-Ch. Nie, Y. Gan, and L. Li, "Analysis of probe-fed conformal microstrip antennas on finite grounded substrate," *IEEE Transactions on Antennas and Propagation*, Vol. 54, No. 2, 554–563, 2006.

25. Rius, J. M., E. Ubeda, and J. Parron, "On the testing of the magnetic field integral equation with RWG basis functions in method of moments," *IEEE Transactions on Antennas and Propagation*, Vol. 49, No. 11, 1550–1553, 2001.

26. Sood, K. K., R. Jyoti, and S. B. Sharma, "A waveguide shunt slot-fed microstrip patch antenna — Analysis using the Method-of-Moments," *IEEE Transactions on Antennas and Propagation*, Vol. 61, No. 11, 5385–5394, 2013.

27. Mikki, S. M. and A. A. Kishk, "Theory and applications of infinitesimal dipole models for computational electromagnetics," *IEEE Transactions on Antennas and Propagation*, Vol. 55, No. 5, 1325–1337, 2007.

28. Sijher, T. and A. Kishk, "Antenna modeling by infinitesimal dipoles using genetic algorithms," *Progress In Electromagnetics Research*, Vol. 52, 225–254, 2005.

29. Liu, X., W. Cai, H. Guo, and H. Yin, "The application of the equivalent dipole-moment method to electromagnetic scattering of 3D objects," *Asia-Pacific Microwave Conference Proceedings*, 3, 2005.

30. Yu, C., J. Yuan, and C. Gu, "Equivalent dipole-moment method for electromagnetic scattering by dielectric bodies," *3rd IEEE International Symposium on Microwave, Antenna, Propagation and EMC Technologies for Wireless Communications*, 924–927, 2009.

31. Schaubert, D. H., D. R. Wilton, and A. W. Glisson, "A tetrahedral modeling method for electromagnetic scattering by arbitrarily shaped inhomogeneous dielectric bodies," *IEEE Transactions on Antennas and Propagation*, Vol. 32, No. 1, 77–85, 1984.

32. Yuan, J., C. Gu, and G. Han, "Efficient generation of method of moments matrices using equivalent dipole-moment method," *IEEE Antennas and Wireless Propagation Letters*, Vol. 8, 716–719, 2009.

33. Rao, S. M., D. R. Wilton, and A. W. Glisson, "Electromagnetic scattering by surfaces of arbitrary shape," *IEEE Transactions on Antennas and Propagation*, Vol. 30, No. 3, 409–418, 1982.

34. Lyon, R. W. and A. J. Sangster, "Efficient moment method analysis of radiating slots in a thick-walled rectangular waveguide," *Proc. Inst. Elect. Eng.*, Vol. 128, No. 4, 197–205, 1981.

35. Cowper, G. R., "Gaussian quadrature formulas for triangles," *In. J. Numer. Meth. Eng.*, 405–408, 1973.

36. Jiade, Y., "A hybrid equivalent dipole moment and adaptive modified characteristic basis function method for electromagnetic scattering by multilayered dielectric bodies," *International Journal of RF and Microwave Computer-aided Engineering*, Vol. 19, 685–691, 2009.

37. Makarov, S. M., *Antenna and EM Modeling with Matlab*, 2002.

38. Balanis, C. A., *Advanced Engineering Electromagnetics*, 2nd Edition, 310–314, 2012.

39. Richmond, J. H., "A reaction theorem and its applications to antenna impedance calculations," *IRE Trans. Antennas Propag.*, Vol. 6, No. 9, 515–520, 1961.

40. Mikki, S. M. and A. A. Kishk, "Theory and applications of infinitesimal dipole models for computational electromagnetics," *IEEE Transactions on Antennas and Propagation*, Vol. 55, No. 5, 1325–1337, 2007.

41. Karimkash, S., A. Kish, and G. Zhang, "Modelling of aperiodic array antennas using infinitesimal dipoles," *IET Micro. Antennas Propag.*, Vol. 6, No. 7, 761–767, 2012.

42. Jinyun, Y., "Symmetric Gaussian quadrature formulae for tetrahedronal regions," *Comput. Meths. Appl. Mech. Engrg.*, Vol. 43, 349–353, 1984.

43. Gilbson, W., *The Method of Moments in Electromagnetic*, 168–175, Chapman&Hall/CRC, Boca Raton, FL, 2008.

44. Yuan, J. and K. Su, "Electromagnetic radiation from arbitrarily shaped microstrip antenna using the equivalent dipole-moment method," *International Journal of Antennas and Propagation*, Vol. 2012, Article ID 181235, 5 pages, 2012.